Symkom 2014 **Open Access**

Aldo Iannetti*, Matthew T. Stickland, and William M. Dempster

An advanced CFD model to study the effect of non-condensable gas on cavitation in positive displacement pumps†

DOI 10.1515/eng-2015-0027
Received Dec 01, 2014; accepted Mar 28, 2015

Abstract: An advanced transient CFD model of a positive displacement reciprocating pump was created to study its behavior and performance in cavitating condition during the inlet stroke. The "full" cavitation model developed by Singhal *et al*. was utilized, and a sensitivity analysis test on two air mass fraction amounts (1.5 and 15 parts per million) was carried out to study the influence of the dissolved air content in water on the cavitation phenomenon. The model was equipped with user defined functions to introduce the liquid compressibility, which stabilizes the simulation, and to handle the two-way coupling between the pressure field and the inlet valve lift history. Estimation of the performance is also presented in both cases.

Keywords: Cavitation; positive displacement pumps; non-condensable gas effect; CFD

1 Introduction

Cavitation in pumps is still a debated topic in technical literature. The main discussed subject focuses on how to correctly estimate the Net Positive Suction Head required (NPSHr) of the device. The reason for the focus on the NPSHr is mainly due to the need to achieve the requirements specified by the API 610, API 674 and DIN EN ISO 13710, where either for Positive Displacement (PD) pump or centrifugal pumps a certain safety margin to avoid cavitation is set. Since pump manufacturers are required to specify the NPSHr, researchers are called to develop tools and procedures to study cavitation in pumps and to estimate accurately the NPSHr. In the case of centrifugal pumps, for instance, many authors, such as Ding [1], have developed a Computational Fluid Dynamics (CFD) based tool to estimate the NPSH curve, in order to find the operating conditions where the drop of 3% in head occurs, as specified by the API. Ding *et al.* also stated that the definition of the NPSHr is affected by the content of air in water. Budris and Mayleben [2] carried out a research oriented at understanding the effect of the air content in water in the estimation of the performance of centrifugal pumps. They found that a small amount of air reduces significantly the suction pressure pulsation, while increasing the amount of air content above a certain threshold delivers no further improvement on the pressure fluctuations, while an increment of the NPSHr occurs.

The case of PD reciprocating pumps appears to be different. The API 674 defines the NPSHr as the NPSH where a decrement of 3% in volumetric efficiency occurs but many authors do not agree in considering the NPSHr in PD pumps a precise engineering requirement. Miller, [3] for instance, stated that any suction pressure above the NPSHr would only improve the performance by increasing the volumetric efficiency and minimizing the effect of the air entrained or dissolved. Other authors such as Opitz and Schlücker [4] presented an experimental study on cavitation in PD pumps indicating that the phenomenon up to a certain limit is harmless, and that strict requirement of the API 674 is perhaps not necessary. In a subsequent study, the same authors [5] discussed the phenomenon of expansion generated cavitation, relating it to the incipient cavitation occurring at the initial stage of the inlet stroke when the plunger of the pump moves backward and the inlet valve is still closed and pushed against its seat by the preloaded spring. This phenomenon will be investigated in more details in this paper.

***Corresponding Author: Aldo Iannetti:** Mechanical and Aerospace Engineering Department, University of Strathclyde, 16 Richmond Street, Glasgow G1 1XQ, Scotland, United Kingdom; Email: aldo.iannetti@strath.ac.uk
Matthew T. Stickland, William M. Dempster: Mechanical and Aerospace Engineering Department, University of Strathclyde, 16 Richmond Street, Glasgow G1 1XQ, Scotland, United Kingdom
† 11^{th} International symposium on compressor & turbine flow systems theory & application areas
SYMKOM 2014 IMP^2, Łódź, 20 – 23 October, 2014

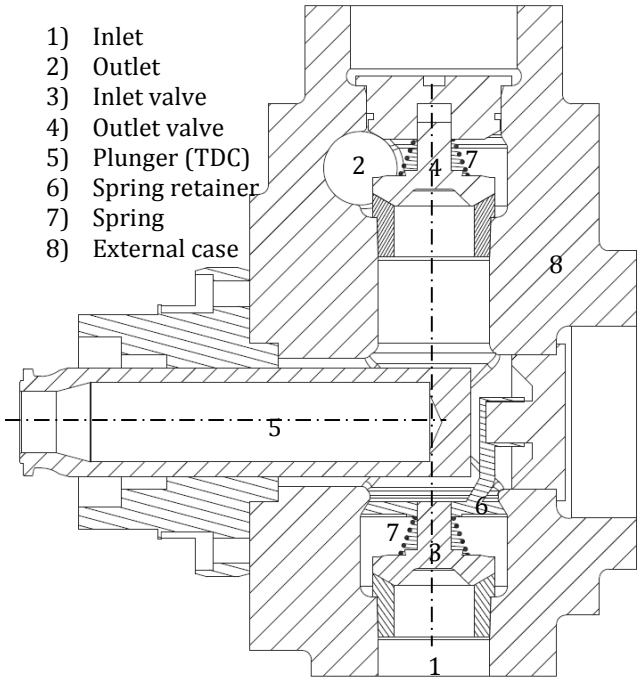

Figure 1: 2D section of the PD pump utilised to create the fluid volume and the mesh for the CFD. Nomenclature is provided.

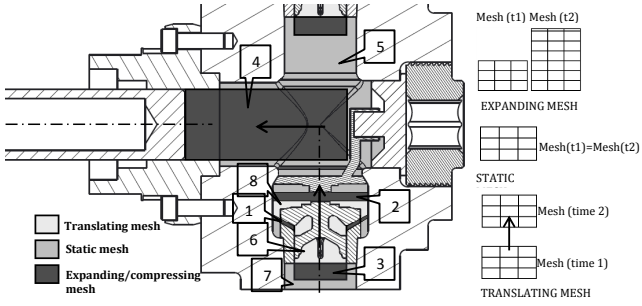

Figure 2: Decomposition pattern of the fluid volumes [9]

The aim of the study being presented is to answer to the following questions:

1. What is the precise effect of the dissolved gas on cavitation in PD pumps?
2. How does it affect the performance of PD pumps?
3. How does it affect the NPSH?

The authors chose to carry out the investigation by means of the advanced CFD model explained and discussed by Iannetti *et al*. [6] that will be briefly recalled in the next sections. The reason for this choice lies on the higher capability of post processing that a CFD solver has over experimental tests. In fact a crucial prerequisite for the analysis shown is to separate the fluid dynamic fields of vapour from that of air, which together constitute the secondary phase. This capability is almost impossible to achieve via experimental investigation.

It is known [7] that clean water at ambient conditions contains 15 ppm (parts per million) of air which is dissolved, as the static pressure lowers during the suction stroke, air separates from the liquid and gathers in bubbles which interact with the pressure field as air is much more compressible than water. It is also known [8] that water contains also a large amount of nuclei which are microscopic bubbles containing water vapour and air and are located in the crevices of the solid boundaries or on dust particles. This amount of gas which is not dissolved may increase the overall amount of air. The interaction non-condensable gas with the pressure field implies an expansion of the former: this phenomenon is usually called gas cavitation. Gas cavitation results in a pressure drop slowdown which may result in a delay of the achievement of the vapour cavitation condition and a mitigation of the water vapour generation.

This work simulates the entire suction stroke of the pump, when the plunger moves backward and the minimum pressure peak is achieved. This paper will discuss the complex phenomena occurring during cavitation via detailed post processing data analysis.

For this purpose, two CFD test cases were created and launched, and their results were compared. The cases dealt with a single chamber PD pump subjected to the same operating and boundary conditions; they differed only in the property of the fluid processed, the first case utilizing water with 15 ppm of dissolved air at standard conditions, while the second case utilised a lower air content of 1.5 ppm.

2 CFD Model, geometry and set-up

The CAD model of a chamber of the PD reciprocating pump shown in Figure 1 was taken in order to create the mesh. The configuration of the pump CAD file, which defined the initial fluid domain of the simulation is shown in the same figure, where the plunger is located at its Top Dead Centre (TDC) position and the valves are closed. As Iannetti *et al*. explained [9], the moving mesh algorithm managed the volume deformation and growth due to valve lift, and the displacement volume increment by means of a transient approach. The numerical analysis was focused on the simulation of the inlet stroke which starts when the plunger is located at the TDC and ends when the inlet valve hits the seat after the plunger gets to the Bottom Dead Centre (BDC). According to theory, the valve should get to the seat

Table 1: Mesh sensitivity analysis test; three mesh sizes were tested [9]

Mesh	Number of Cells [M]	Average Skewness [-]	Approx computational time [h]
1	3	0.24	48
2	5	0.26	60
3	6	0.22	72

Table 2: Mesh 2 details summar

Location (see figure 2)	Volume descriprion	Mesh type	Size details min-max [mm]	Mesh motion
1	Valve-seat lift volume	Hexahedral	0.2–1	Expanding (layering)
2	Inlet valve downstream	Wedge	1–3	Compressing (layering)
3	Inlet valve upstream	Hexahedral	2–3	Expanding (layering)
4	Displacement volume	Hexahedral	2.5	Expanding (layering)
5	Pump chamber	Tetrahedral	2.5–5	Static
6	Valve internal	Tetrahedral	1–2.5	Translating
7	Inlet manifold	Tetrahedral	2–4	Static
8	Valve top volume	tetrahedral	1–2	Translating

as soon as the plunger gets to the BDC, however, because of valve inertia, the operating conditions and the fluid properties, there could be a delay in the inlet valve closing time, which would extend the inlet stroke overlapping the first stage of the outlet stroke. This has been observed by Iannetti *et al*. [6] but the influence of the air content on it is still unclear.

Solid volumes were utilised to generate the fluid volumes by means of Boolean operations; they were subsequently meshed. The choice of the mesh type was made according to the decomposition pattern needed by the moving mesh technique. The process is explained by Iannetti *et al*. [9] for a slightly different geometry but, since the basis hypothesis did not change, the pattern is proposed again as illustrated in Figure 2.

The static and translating volumes were meshed utilizing tetrahedral cells. Expanding/compressing volumes were crucial to simulate the growth of the displacement volume as well as the growth of the valve lift volume located between the valve and the seat (valve-seat gap volume); they were either a cylindrical or annular shaped and were meshed utilizing hexahedral cells so that the expansion/creation of cell layers could affect the height of the parallel cell layers (layering technique [9]). The mesh spacing was decided after a mesh sensitivity analysis, which fixed it as the optimum between the low computational time and high accuracy needs. As explained by Iannetti *et al*. [9], for this analysis three mesh sizes were tested (Table 1). Meshes 2 and 3 provided the same results, which were more accurate than the ones provided by mesh 1; the latter was also affected by numerical instability. It was decided to carry on the analysis utilizing mesh 2, as it reduced the computational efforts. The details of mesh 2 are shown in Table 2.

The Singhal *et al*. [11] cavitation model was chosen along with the solver settings and sub-models shown in Table 1. A User Defined function (UDF) was written and attached to the CFD solver in order to manage the two-way coupling between the valve lift and the chamber pressure field. Figure 3 shows the steps performed by the UDF and how it interfaces to the main numerical solver. A second UDF was written to include the liquid compressibility effects which were of great importance to stabilize the simulation in the instants within the pumping cycle when inlet and outlet valve were both closed; the governing equations have been discussed by Iannetti *et al*. [9].

A mass dependent inlet pressure was chosen to account for the complex shape of the inlet pipeline. The pump model boundary was five inlet pipe diameters upstream of the inlet valve and the remaining part of the pipe was simulated by means of separated steady state simulations with 5 kg/s to 30 kg/s mass flow. For each of these analyses the pressure drop across the ends of the pipe was taken to build the curve shown in Figure 4. The curve was fed by means of piecewise linear law into the main model of the pump in order to obtain a mass flow adjusted pressure inlet condition from a constant level chosen as 0 PaG.

Table 3: Solver settings summary

Solver		RANS, pressure based, transient	
Models	Multiphase	Mixture model [10]	
		Phases	Water liquid — Primary phase
			Water vapour — Secondary phase
	Turbulence	K-ε Standard	Enhanced wall treatment
	Cavitation	Singhal *et al.* [11]	15 ppm air (Case 1), 1.5 ppm (Case 2)
Pressure-Velocity coupling		SIMPLE	
Spatial discretization		Momentum	Second order upwind
		Vapour	First order upwind
		Turbulent kinetic energy	Second order upwind
		Turbulent dissipation rate	Second order upwind
Transient formulation		First order implicit	
Under relaxation factors		Pressure	0.3
		Momentum	0.7
		Vapour	0.5
		Turbulent kinetic energy	0.8
		Turbulent dissipation rate	0.8
Residuals		10^{-3}	
Time step		0.125° crank rotation $\equiv$ 1.6×10^{-4}s @130 rpm	
Max Iteration per time step		35	
UDFs		Compressibility of water [9]	
		Valve dynamics	

Table 4: Inlet pressure boundary and initial conditions for both cases under investigation

Case	Pressure: function of the mass flow rate Inlet pressure [kPaG]	Chamber initialization pressure [kPaG]
Case 1 and 2	0 - ΔP (see Figure 4)	0

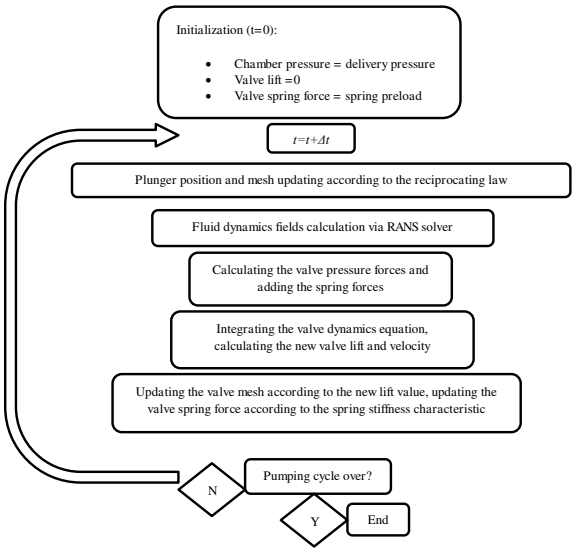

Figure 3: User Defined Function to drive the valve motion, how it relates to the main CFD solver (Iannetti, Stickland, and Dempster 2015)

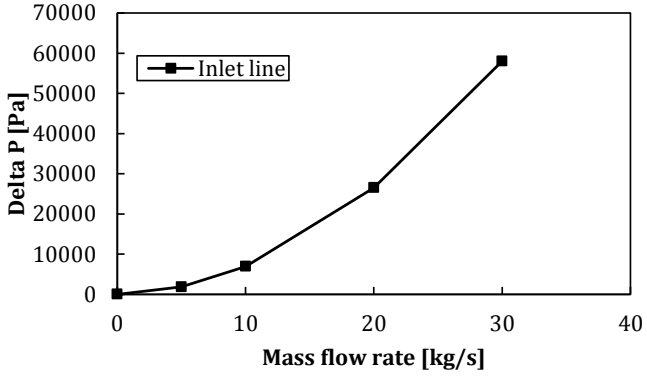

Figure 4: Inlet pipe pressure drop Vs mass flow characteristic. The points of the curve were simulated by means of a separated steady-state CFD analysis of the inlet pipe only.

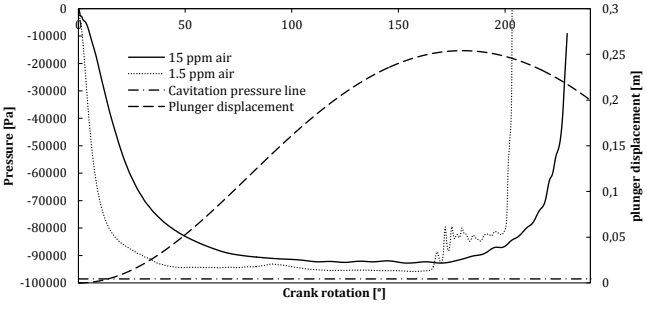

Figure 5: Pump chamber pressure history. A liquid poorer in air mass fraction is affected by a higher pressure drop.

The initial and boundary conditions are summarized by Table 4.

An Intel Xeon CPU W3670 @3.2GHz CPU (6 cores) was employed for the simulations. Approximately 10 days was the calculation time needed for each case.

3 Numerical results and discussion

Figure 5 shows the time history of the chamber static pressure throughout the inlet stroke for both cases of air mass fractions of 15 and 1.5 ppm. The pressure monitor point was a static point close to the TDC plunger position. The simulations showed that the lower the air content, the closer is the minimum chamber pressure to the cavitation pressure. Figure 5 also shows that in case of lower air content, the pressure drops more quickly than in the first case, and this results in a low pressure regime that lasts longer and increases the generation of vapour as shown in Figures 6 and 7.

Figure 6 shows the situation in terms of secondary phase (air + water vapour) volume fraction in the valve-seat volume throughout the inlet stroke. An important remark that has to be pointed out is how the secondary phase volume fraction is actually divided in terms of vapour and air. The left plot of Figure 6 shows the higher secondary phase fraction of the first case (solid line, 15 ppm air mass fraction) but the middle plot demonstrates that the vapour generation was higher in case 2 (1.5 ppm) at ~25% versus ~16%. Therefore it can be said that case 1 is affected by a higher air expansion rather than vapour generation. Furthermore, while in the first case air and vapour fractions were evenly ~16% for both, in the second case the difference between vapour and air is significant (~25% versus ~2.5% respectively).

Figure 7 shows the secondary phase volume fraction in the vicinity of the plunger top surface throughout the inlet stroke. The plunger region was more affected by a lower vapour volume fraction than the valve region. For instance, considering case 1 (15 ppm), the maximum secondary phase volume fraction was circa 32% (valve-seat gap volume, Figure 6 left); close to the plunger the amount was 19% (Figure 7 left). Furthermore, near the plunger the liquid richer of air showed an uneven subdivision of air and vapour volume fraction, respectively 6% and 13% (solid line, Figure 7 middle and right). Case 2, on the other hand, showed an even subdivision of circa 2.5% air and vapour.

The trends of Figures 6 and 7 are confirmed by the secondary phase chamber volume integral, depicted in Figures 8 and 9. When operating with a 15 ppm air mass fraction liquid, the pump shows twice the integral of the sec-

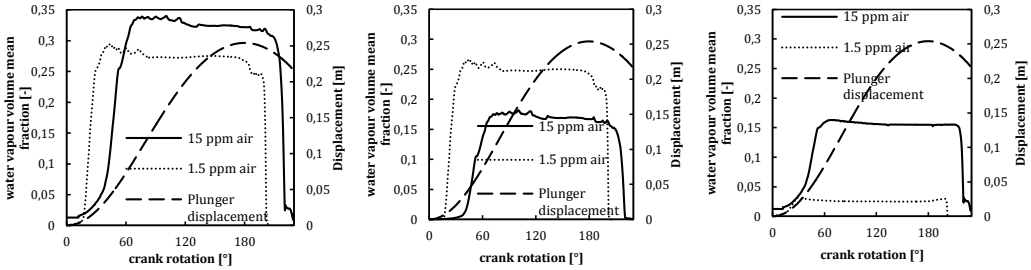

Figure 6: (Left) 2nd phase (water + air) volume fraction in the valve-seat lift volume when the air mass fraction is 15 and 1.5 ppm. (middle) Overall amount of vapour volume fraction. (right) overall amount of air volume fraction.

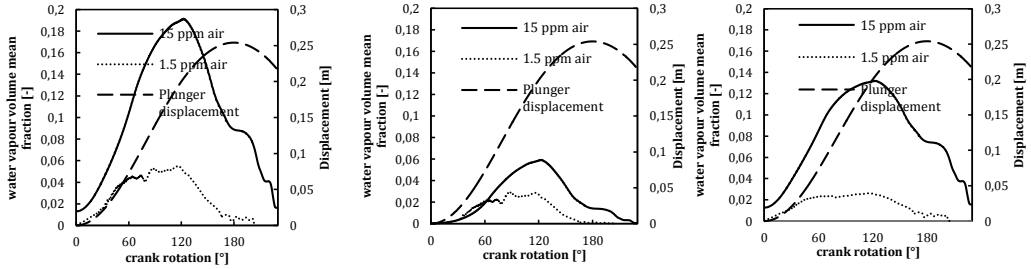

Figure 7: (Left) 2^{nd} phase (water + air) volume fraction in the vicinity of the plunger when the air mass fraction is 15 and 1.5 ppm; (middle) Overall amount of vapour volume fraction; (right) overall amount of air volume fraction.

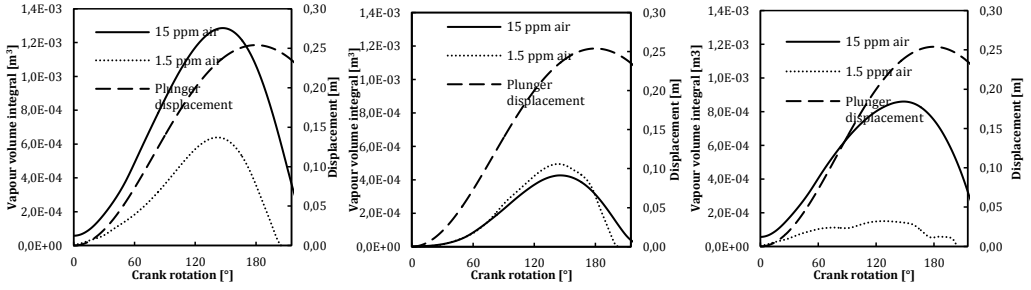

Figure 8: (left) Chamber volume integral of the 2^{nd} phase (vapour + air), when air mass fraction is 15 ppm (case1) and 1.5 ppm (case2); (middle) Chamber volume integral of vapour; (right) Chamber volume integral of air.

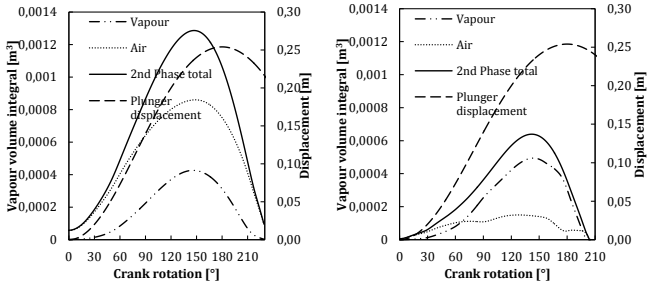

Figure 9: (left) Chamber volume integral of the second phase components Case number 1, air mass fraction 15 ppm; (right) Case number 2, air mass fraction 1.5 ppm.

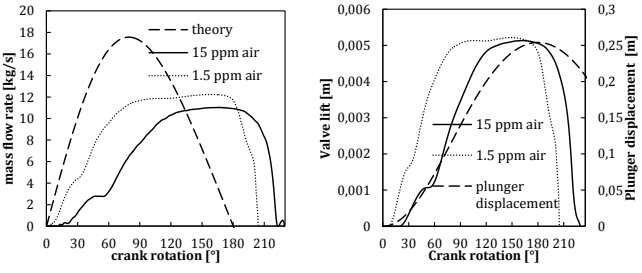

Figure 10: (left) mass flow rate throughout the inlet stroke when the air mass fraction is 15 and 1.5 ppm; (right) valve lift history.

ondary phase volume (1.28 l versus 0.64 l) but in large part the secondary phase is composed of air rather than vapour (respectively 0.86 l against 0.42 l, Figure 8 middle and right). The case of 1.5 ppm of air mass fraction shows a slightly higher vapour volume integral (0.49 l versus 0.42 l) and a much lower air volume integral (0.15 l against 0.49 l of vapour).

Table 5: Pump performance estimation summary; comparison of the two fluid properies 15 ppm vs 1.5 ppm air mass fraction

	Air mass fraction [ppm]	Volumetric efficiency Vs standard conditions [%]	Inlet valve opening time [°]	Inlet valve closing time [°]
Case 1	15	78.5	12	229
Case 2	1.5	95	4	205

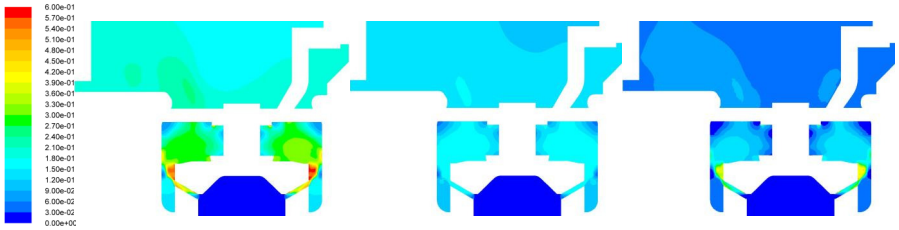

Figure 11: Case 1 (15 ppm air mass fraction) at 120° of crank rotation: (left) total second phase volume fraction; (middle) air volume fraction; (right) vapour volume fraction.

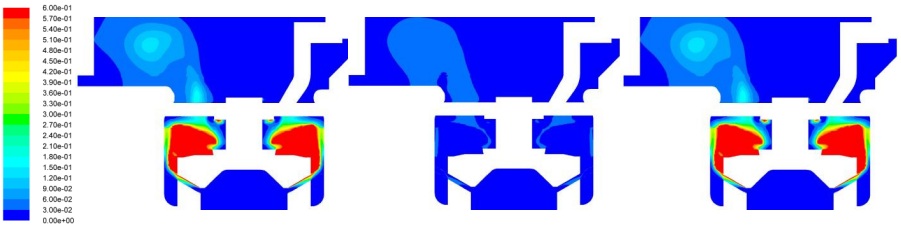

Figure 12: Case 2 (1.5 ppm air mass fraction) at 120° of crank rotation: (left) total second phase volume fraction; (middle) air volume fraction; (right) vapour volume fraction.

Table 5 summarises and quantifyies the performance of the pump. In both cases studied, th evolumetric efficiency loss was higher than 3% but case 1 showed a much lower volumetric efficiency (78.5% against 95%) because of the much higher air content which demonstrated a great influence in the performance deterioration. Table 5 also shows that the higher is the volumetric efficiency loss, and the bigger is the inlet valve closing delay (the theory indicates the end of the inlet stroke at 180° of shaft rotation). This can be explained by the time needed for the plunger to compress the secondary phase to convert it (by dissolution) to liquid phase. Furthermore a higher air content resulted in a bigger inlet valve opening delay (12° against 4°) because of the capability of air of expanding and slowing down the chamber pressure drop.

Figure 10 shows the mass flow rate (left) and inlet valve lift (right) trends of the two cases under investigation. The mass flows are compared to the theory curve, which is calculated considering a one phase incompressible fluid with zero inertia inlet valve (diplacement volume times the density of water at standard condition). Case 2 shows an average mass flow rate higher than case 1, which explains the higher volumetric efficiency. The valve lift plot shows clearly the difference in closing delay highlighted in Table 3.

Figures 11 and 12 show the contour of the secondary phase volume fraction respectively for cases 1 and 2. Both figures represent an image taken when the plunger rotation was 120°, which is close to the maximum vapour peak generation for both of cases. The contours confirm what was already stated in the discussion of Figure 5 to 10. Vapour is generated mainly in the valve-seat gap volume and propagates afterwards. According to the CFD simulation and supported by Figure 11, the expansion provided by the plunger generates a wide region where the air comes out of the fluid phase as dissolved gas and expands randomly around the plunger. This phenomenon is known as gas cavitation and was observed by Opitz and Schlücker [4]. As the amount of air mass fraction was very low, case 2 showed the typical features of vapour cavitation (Figure 12) whereby the secondary phase is concentrated in the vicinity of the valve, where it is mainly generated.

4 Conclusion

A transient and comprehensive CFD model of a one-chamber PD pump was created to estimate the performance of the device under different working fluid properties. Two cases were investigated; in case 1 water with 15 ppm of air mass fraction content was considered, while case 2 dealt with a 1.5 ppm air mass fraction dissolved. The operating conditions (i.e. shaft angular speed and inlet pressure) were designed to achieve the full cavitating conditions so that the effect of the non-condensable gas mass fraction content on cavitation could be investigated. The CFD model made use of the Singhal *et al.* cavitation model [11], the multiphase mixture model [10, 12] and two UDFs modelled the compressibility of the fluid and the two-way coupling between the valve lift and the pressure field. The valve spring effect and the valve inertia were also taken into account. A complete inlet stroke was simulated, from the initialization point (plunger located at the TDC) untill the end of the valve lift history. The two cases, in fact demonstrated a different dynamics and in case 2 the valve ended the lift sooner than case 1.

General remarks on cavitation

According to the CFD model and under the investigated operating conditions, the plunger expansion created the pressure drop needed for the vapour cavitation to appear but the air expansion (gas cavitation) prevented the vapour formation in the vicinity of the plunger which was affected by the vapour previously generated by the valve rather than that generated by the plunger itself. Once the average static pressure in the chamber ranged around the vapour pressure, and the flowing velocity in the valve-seat gap volume exceeded a certain treshold, vapour cavitation appeared and affected primarily the lift volume; it moved downstream towards the plunger afterwards. The triggering cause of cavitation was the high flow velocity (flow induced cavitation [4]) rather than the expansion cavitation which appeared to be just a prerequisite.

Influence of the non-condensable mass fraction on cavitation

Non-condensable gas mass fraction influences the chamber pressure history (Figure 5), the dissolved air slows down the pressure drop while it comes out of the liquid and expands. Air expansion tends to fill the void left by the plunger at the beginning of the inlet stroke when the valve is closed and delays vapour cavitation appearance. Case 1, which deals with a higher gas content fluid, shows a lower vapour volume integral than case 2, which deals with a lower air content (Figures 8 and 9). On the other hand the air content is itself a source of volumetric efficiency loss as shown by Table 3. Figure 9 demonstrates that the overall secondary phase content (vapour and air) defines the volumetric efficiency rather than the vapour content itself; in fact, case 1, which shows the highest secondary phase volume integral, also shows the lowest veolumetric efficiency. Figure 5 demonstrate also that the higher the air content, the higher the minimum pressure (absolute value), this provides a further safety factor on cavitation and increases the NPSH of the pump.

The analisys demonstrated the importance of the working liquid properties for an accurate estimation of the performance of the pump as well as the prediction of the cavitation damage. Although the overall content of air (dissolved air plus the nuclei content) is not harmful for the pump, taking into account the non-condensable air mass fraction in cavitation results in a better estimation of the vapour volume fraction prediction. Despite air cavitation, vapour bubbles can harm the pump significantly. An accurate prediction of the amount and the location may result in a better understanding of the design and operating parameters affecting cavitation and this implies a reliable support for pump designers and manufacturers.

Future improvement of the analysis presented in this paper is planned, the authors are currently working on a test rig to valdidate the CFD data herein presented.

References

[1] H. Ding, F. C. Visser, and Y. Jiang, A practical approach to speed up NPSHR prediction of centrifugal pumps using CFD cavitation model, in Proceedings of the ASME 2012 Fluids Engineering Summer Meeting., 2012, p. Paper No. FEDSM2012–72282.

[2] A. R. Budris and P. A. Mayleben, Effects of entrained air, NPSH margin, and suction piping on cavitation in centrifugal pumps, in Proceeding of the 15th international pump users symposium, 1998, pp. 99–108.

[3] J. E. Miller, The reciprocating pump, theory design and use, Second Edi. Krieger publishing company, 1995.

[4] K. Opitz and E. Schlücker, Detection of Cavitation Phenomena in Reciprocating Pumps using a High-Speed Camera, Chem. Eng. Technol., vol. 33, no. 10, pp. 1610–1614, Jul. 2010.

[5] K. Opitz, E. Schlücker, and O. Schade, Cavitation in reciprocating positive displacement pumps, in Twenty-seventh international pump users symposium, 2011, pp. 27–33.

[6] A. Iannetti, M. T. Stickland, and W. M. Dempster, A CFD study on the mechanisms which cause cavitation in positive displace-

ment reciprocating pumps, J. Hydraul. Eng., vol. 1, no. 1, pp. 47–59, 2015.
[7] G. Kuiper, Cavitation in ship propulsion, Delft: Delft University of Technology, 2010.
[8] P. Eisenberg, Cavitation Damage, Office of Naval Research, 1963.
[9] A. Iannetti, M. T. Stickland, and W. M. Dempster, A computational fluid dynamics model to evaluate the inlet stroke performance of a positive displacement reciprocating plunger pump, Proc. Inst. Mech. Eng. Part A J. Power Energy, vol. 228, no. 5, pp. 574–584, Apr. 2014.
[10] ANSYS, ANSYS Fluent Theory Guide, vol. 15317, no. November, ANSYS Fluent, 2011.
[11] A. Singhal and M. Athavale, Mathematical basis and validation of the full cavitation model, J. Fluids Eng., vol. 124, no. 3, p. 617, 2002.
[12] ANSYS, ANSYS FLUENT User's Guide, vol. 15317, no. November. ANSYS Inc., 2011.